Nanotechnology **24** (2013) 265707 (13pp) doi:10.1088/0957-4484/24/26/265707

Lateral bending of tapered piezo-semiconductive nanostructures for ultra-sensitive mechanical force to voltage conversion

Rodolfo Araneo[1] **and Christian Falconi**[2,3]

[1] DIAEE—Electrical Engineering Division, 'Sapienza' University of Rome, Via Eudossiana 18, 00184, Rome, Italy
[2] Department of Electronic Engineering, University of Rome 'Tor Vergata', Via del Politecnico 1, 00133, Rome, Italy
[3] CNR IDASC, Via Fosso del Cavaliere, 100, 00133 Rome, Italy

E-mail: falconi@eln.uniroma2.it

Received 14 February 2013, in final form 23 April 2013
Published 4 June 2013
Online at stacks.iop.org/Nano/24/265707

Abstract
Quasi-1D piezoelectric nanostructures may offer unprecedented sensitivity for transducing minuscule input mechanical forces into high output voltages due to both scaling laws and increased piezoelectric coefficients. However, until now both theoretical and experimental studies have suggested that, for a given mechanical force, lateral bending of piezoelectric nanowires results in lower output electric potentials than vertical compression. Here we demonstrate that this result only applies to nanostructures with a constant cross-section. Moreover, though it is commonly believed that the output electric potential of a strained piezo-semiconductive device can only be reduced by the presence of free charges, we show that the output piezopotential of laterally bent tapered nanostructures, with typical doping levels and very small input forces, can be even increased up to two times by free charges.

Our analyses confirm that, though not optimal for piezoelectric energy harvesting, lateral bending of tapered nanostructures with typical doping levels can be ideal for transducing tiny input mechanical forces into high and accessible piezopotentials. Our results provide guidelines for designing high-performance piezo-nano-devices for energy harvesting, mechanical sensing, piezotronics, piezo-phototronics, and piezo-controlled chemical reactions, among others.

(Some figures may appear in colour only in the online journal)

Quasi-1D piezoelectric nano-devices can find applications in sensors, actuators, energy harvesting [1], piezotronics [2], piezo-phototronics [2], and piezo-controlled chemical reactions [3], among others. In fact, compared with conventional piezoelectric materials, quasi-1D piezoelectric nanostructures can be significantly deformed by smaller mechanical forces, have higher piezoelectric coefficients [4, 5], and exhibit outstanding mechanical properties [5], including substantially higher fracture strains [5, 6].

However, despite impressive progress [2, 7–13] reported in just a few years from the first piezoelectric nanogenerators [1, 14], existing piezoelectric nano-devices are obviously sub-optimal, primarily due to the complexity of modeling, fabricating, characterizing, and packaging devices at the nanoscale. Additionally, the electro-mechanical characterization of piezoelectric nanostructures is still a challenge [5]; for instance, though the dependence of the resonance frequency of a free-standing ZnO nanowire on the amplitude of the exciting AC voltage has been solidly attributed to piezoelectricity [15, 16], in the absence of an accurate quantitative model it is not yet possible to take advantage of such a dependence to extract key parameters such as doping level, piezoelectric coefficients, and Young modulus. For all these reasons, substantial efforts are being devoted to improving both the theoretical understanding and numerical modeling of piezo-nano-devices [17–23].

In particular, under the assumption of negligible free charges, FEM simulations have shown that vertical compression is better than lateral bending from both the points of view of high output voltages and mechanical-to-electrical energy transduction capabilities [19], which also seem consistent with the high piezopotentials experimentally generated by vertical compression [9, 13, 24]. In fact, different from vertical compression, which results in a practically uniform strain within the nanowire, in the case of lateral bending the base of the nanowire (i.e. the region where the strain is maximum and, therefore, the region which could be the best for generating high piezopotentials) is partially deactivated by the highly conductive seed layer at the base of the nanowire, [19] which forces a close-to-zero voltage difference at the base. In fact, subsequent theoretical efforts [21, 22] and energy harvesting devices [7, 9, 10, 12] have used vertical compression. However, remarkably, all previously reported theoretical studies on lateral bending [17–20, 23] were restricted to piezoelectric nanostructures with constant cross-sections, such as cylindrical/rectangular/hexagonal nanowires [17–20, 23] or rectangular nanowalls (nanosheets) [19, 23].

As to experimental studies, there are numerous reports on the lateral deflection of piezoelectric nanowires [1, 25–36], but only very few [32, 37] have considered tapered nanostructures and, in all cases, the crucial implications of the tapered shape have never been discussed. In a previous paper [32], lateral bending of tapered nanostructures with likely high doping levels still resulted in rather high AFM recorded potentials; however, nanostructures with very different shapes were compared without discussing the effects of the tapered geometry. In another work [37] the authors measured, with ZnO nano-needles, voltage peaks with magnitudes up to 35 mV, which is close to the record values obtained with a certain sample containing constant-cross-section ZnO nanowires [36] and much higher than values, e.g. always below 9 mV, obtained on different samples containing constant-cross-section ZnO nanowires under similar mechanical excitations [1, 36]; nevertheless, the importance of the tapered shape was not discussed. We also stress that, though interesting, the AFM experiments on tapered piezoelectric nanostructures [32, 37] do not allow a fair comparison between constant cross-section and tapered geometries because the electric potentials recorded by AFM tips are likely very small fractions of the piezopotentials [1] (the measured voltage peaks, often just a few mV [1], are originated by piezopotentials sufficient for effectively forward-biasing Schottky junctions [1, 17, 18, 20]) and are substantially reduced by parasitic contact resistances and capacitances as well as by the fast sliding process; moreover, all these problems are likely exacerbated in the case of nano-needles [37] or nano-cones [32] due to the much smaller contact area and to the even faster sliding process.

In summary, there are no studies on the piezopotential in laterally bent tapered nanostructures, nor discussions on their potentially crucial advantages; moreover, until now, when tapered nanostructures have been used in experiments [32, 37], the critical role of the geometry has not been recognized.

Recently, it has been shown that vertical compression of piezo-semiconductive nanowires with truncated conical shapes can provide significant advantages [22]; in practice, if the tip of the nanowire is sharp enough, a much larger strain is generated at the tip and results in much higher piezopotentials. In fact, the piezopotential is almost the same as would be obtained in a very thin cylindrical nanowire having the same diameter as the small tip of the truncated conical nanowire; however, obviously, the tapered nanowire offers superior mechanical robustness, including a much stronger adhesion to the substrate, and is less subject to buckling, thus permitting the application of higher almost-ideal vertically compressive strains, which may also be a key for efficient mechanical-to-electrical transduction (in a compressed piezoelectric nanowire, the ratio between the stored electrostatic energy and the total stored energy increases with increasing compressive strain [22]). Besides, the piezoelectric coefficients can be significantly increased by downscaling, and it has even been predicted that an escalation of up to two orders of magnitude of the piezoelectric coefficients may be achieved if the diameter of a piezoelectric nanowire can be reduced down to 1 nm [4, 5]; however, if the diameter must be reduced to such small dimensions a constant cross-section may not offer sufficient mechanical robustness and stability, so that tapered nanostructures could be preferable. Nevertheless, until now the piezoelectric potential of tapered nanowires has only been studied in the case of vertical compression [22] and the only reported comparison between vertical compression and lateral bending [19] has taken into account nanostructures with constant cross-section and without free charges (which is obviously a very crude approximation).

Here, by using FEM calculations and taking into full account free charges, we confirm that vertical compression is likely more effective for energy harvesting, but also show that laterally bent tapered nanostructures can actually be ideal for transducing minuscule mechanical forces into high and accessible piezopotentials. Moreover, we show that, contrary to superficial expectations, laterally bent conical doped nanowires can give even higher output piezopotentials than hypothetical perfectly dielectric nanowires. Our results can provide guidelines for designing high-performance piezo-nano-devices for piezotronics, piezo-phototronics, piezo-controlled chemical reactions, as well as for the electro-mechanical characterization of piezoelectric nanostructures.

1. Results and discussion

1.1. Lateral bending of constant cross-section and tapered piezoelectric nanowires

Most theoretical and experimental studies on piezo-nano-devices have focused on zinc oxide (ZnO) because of its many advantages, including: biocompatibility; semiconductive properties; large direct band gap; high exciton binding energy; high piezoelectric coefficients; pyroelectricity; richness of geometries; simple, low-cost, low-temperature, CMOS/MEMS compatible processing by wet chemistry.

Therefore, though our results can be easily extended to other materials, we have also chosen ZnO as a representative piezo-semiconductive material.

Figure 1 schematically shows the cylindrical and truncated conical nanowires used in our simulations, the coordinate system, and the fixed constraint $\mathbf{u} = 0$ at the base, where $\mathbf{u}$ is the displacement vector. Unless otherwise noted, the dimensions of the nanowires are as follows: the cylindrical nanowire has radius, R_{nw}, and length, L_{nw}, equal to 150 nm and 4 μm, respectively; the truncated conical nanowire has base radius, $R_{b,nw}$, tip radius, $R_{t,nw}$, and length, L_{nw}, equal to 150 nm, 25 nm, and 4 μm, respectively. In all our simulations, in order to avoid punctual forces [17, 18, 20], the nanowires are laterally deflected or vertically compressed by a force which is uniformly applied at the entire tip surface; furthermore, in the case of lateral bending the piezopotential is taken at the cross-section $z = 3.8$ μm, i.e. at a distance of 200 nm from the tip, so that distortions due to the method (i.e. force uniformly applied at the tip surface) are negligible, similar to previous lateral bending calculations [17–19]. Unless otherwise noted, the magnitude of the lateral bending or vertical compressive force is 442 nN. In fact, for the sake of comparison, the reference values for both the dimensions of the nanowires (R_{nw}, L_{nw}, $R_{b,nw}$, $R_{t,nw}$) and the magnitude of the force (442 nN) are identical to the reference values used in previous FEM calculations on vertically compressed nanowires with both cylindrical [21, 22] and truncated conical [22] shape. For consistency with previous analyses, we just consider an ideally conductive seed layer [17–20, 23]. Similar to previous FEM analyses [17–22], for simplicity, we assume perfect Ohmic contacts between the nanowire and the electrodes. In tapered nanostructures, the piezoelectric coefficients at the tip can be substantially increased by the small dimensions [4, 5]; for consistency with all previous investigations and in the absence of accurate experimental values we prefer not to consider such size effects which may further favor tapered nanostructures. We also mention that there are several techniques for synthesizing tapered piezoelectric nanostructures [37–41], including, for instance, a simple procedure for synthesizing ZnO nanotips with diameter of the tips around 10 nm [39].

Figure 2 shows the color plots of the piezoelectric potential at the cross-section $z = 3.8$ μm (circular color-maps) and at the cross-section $x = 0$ (bent nanowires color-maps) for both the cylinder and the truncated conical nanowires, for both n-type and p-type doping, with dopant concentrations N_D equal to 10^{17} cm^{-3} (in both the n-type and p-type simulations) and with a temperature equal to 300 K. For graphical clarity the color scale bars are saturated (i.e. no color changes above a certain upper threshold and below a certain lower threshold) when a linear color scale would not permit one to appreciate the voltage differences within the body of the nanowire.

Importantly, the minimum and maximum values of the piezopotential in the deflected cylindrical nanowires are found in very small and internal (i.e. not accessible from an outside contact) portions of the bent nanowire and are, therefore, practically inaccessible; for instance, if we consider the n-type deflected cylindrical nanowire, the minimum value of the piezopotential is −229.6 mV, but is found in an internal region, close to the base of the nanowire (where the maximum strain is present), and is, therefore, not practically accessible; in fact, the minimum value of the piezopotential which can actually be extracted from the nanowire is found at the tip and is around −5.9 mV (see the color plot for the cross-section $z = 3.8$ μm). This problem is absent in the tapered configurations; for instance, the minimum potential in the laterally bent n-type conical nanowire is −2.126 V and is found exactly at the tip of the tapered nanostructures, i.e. is accessible.

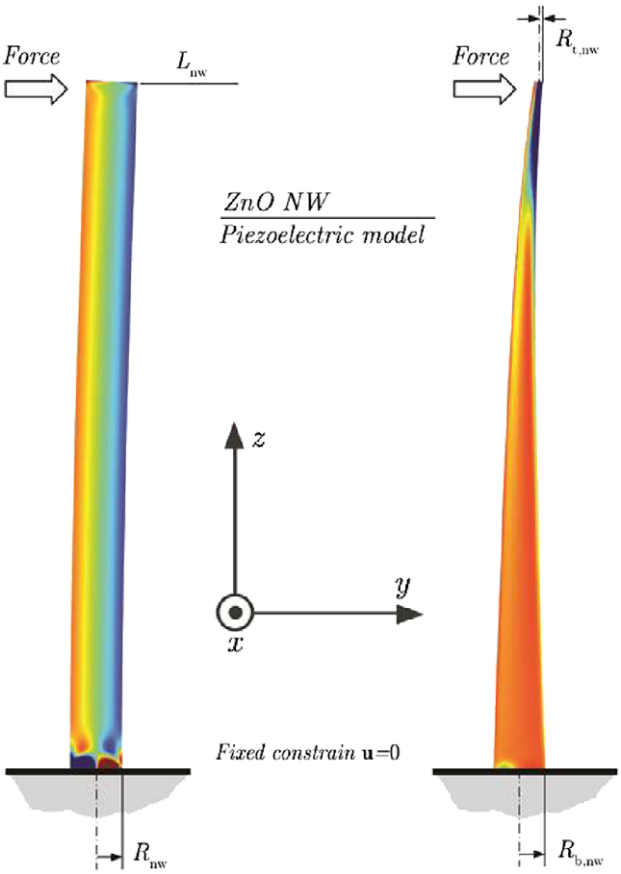

Figure 1. Coordinate system and schematic representation of the cylindrical and truncated conical nanowires with the definitions of R_{nw} (radius) and L_{nw} (length) for the cylindrical nanowire and of $R_{b,nw}$ (base radius), $R_{t,nw}$ (tip radius), and L_{nw} (length) for the truncated conical nanowire.

There are two reasons for the much larger piezopotentials found at the tip of tapered nanostructures: first, in comparison with constant-section nanostructures, the tapered shape mechanically allows one to generate much higher strains at the tip, and, second, such high strains are effectively transduced into high piezopotentials because the tip is far from the total bottom contact [19] constituted by the highly conductive seed layer and, therefore, its strain can be effectively converted into a piezopotential. As a result, the magnitudes of the 'extreme' potentials in the tapered nanowire are much higher (e.g. around 2 V in our case) and, a crucial advantage, easily accessible; in contrast, the accessible potentials in the cylindrical nanowires are orders of magnitude lower (e.g. around 5 mV in our case).

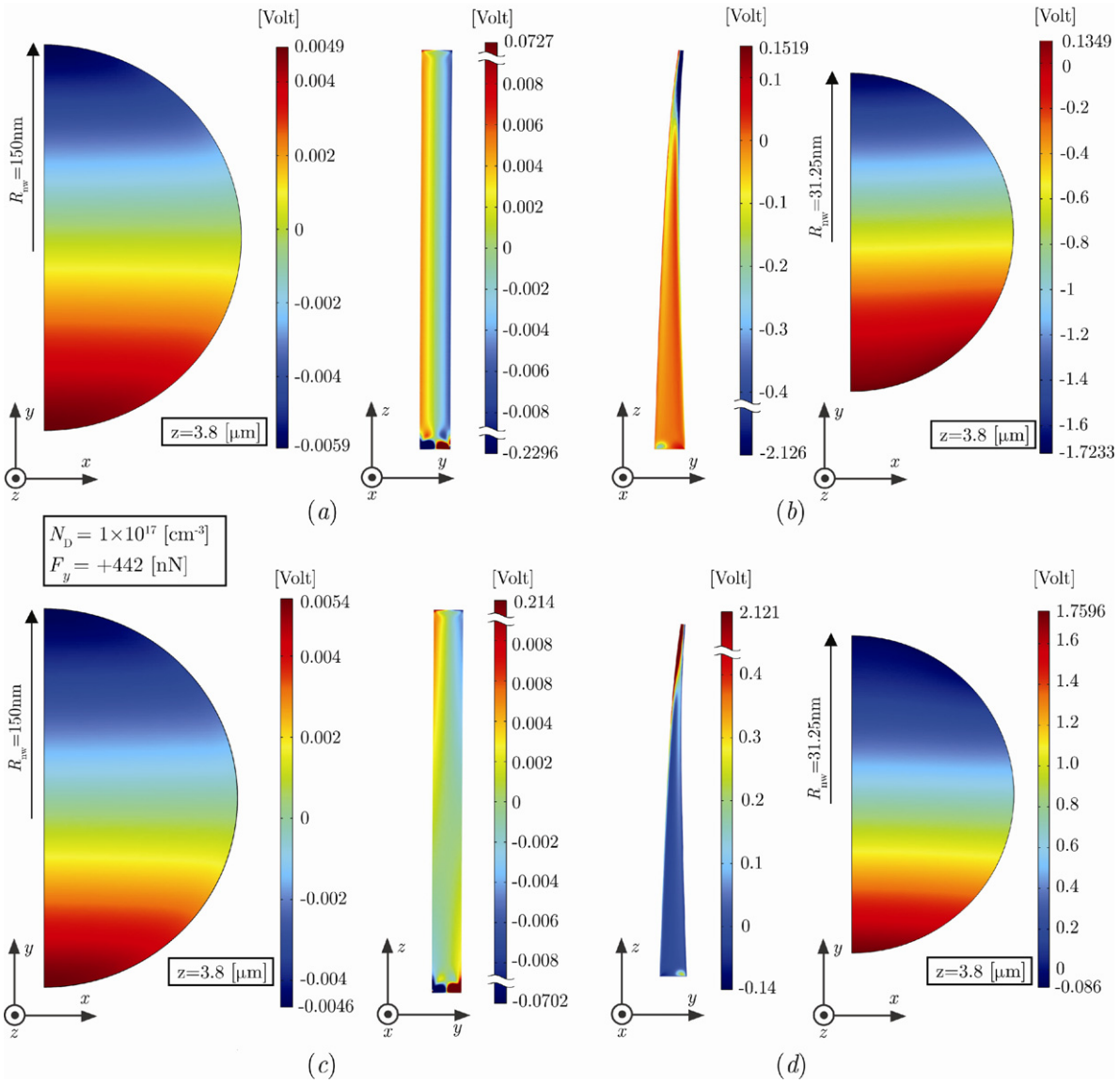

Figure 2. Color-maps of the piezopotential in laterally bent cylindrical and truncated conical ZnO nanowires for both the cross-sections $z = 3.8$ μm and $x = 0$ with dopant concentration $N_D = 10^{17}$ cm^{-3}, $T = 300$ K, and lateral force, $F_y = 442$ nN, for both n-type and p-type doping; for graphical clarity some color bars are saturated (see text). (a) Piezopotential at both the cross-sections $z = 3.8$ μm and $x = 0$ for an n-type cylindrical nanowire. (b) Piezopotential at both the cross-sections $z = 3.8$ μm and $x = 0$ for an n-type truncated conical nanowire. (c) Piezopotential at both the cross-sections $z = 3.8$ μm and $x = 0$ for a p-type cylindrical nanowire. (d) Piezopotential at both the cross-sections $z = 3.8$ μm and $x = 0$ for a p-type truncated conical nanowire.

Consistently with [18], figure 2 also shows that in n-type nanowires the positive piezopotential in the extended regions is effectively screened by the negative free charges, electrons; in contrast the negative piezopotential in the compressed region cannot be screened because the free charges, electrons, are repelled by negative potentials. By duality, in p-type nanowires, the free charges, holes, can only effectively screen the negative piezopotential in the compressed region and the positive piezopotential is preserved. The small differences between the maximum magnitudes of the piezopotentials in n-type and p-type nanowires are due to the small asymmetries between holes and electrons (different effective masses). For conciseness, in the following we restrict ourselves to n-type doping only, because ZnO nanowires typically exhibit n-type doping and p-type nanowires are more difficult to synthesize [29]. However, we stress that p-type doping may also offer important practical advantages; for instance, if a p-type nanowire is laterally deflected by a contacting AFM tip or other structures [29], the piezopotential with high magnitude can be extracted directly by the contacting structure rather than from the opposite side (as is the case for n-type nanowires), which is obviously a crucial difference for practical applications. Anyway, due to the small and predictable (inversion of the sign of the piezopotential and of the regions with high magnitudes of the piezopotential) differences between n-type and p-type doping, our results, with obvious modifications, can also be applied to p-type doping.

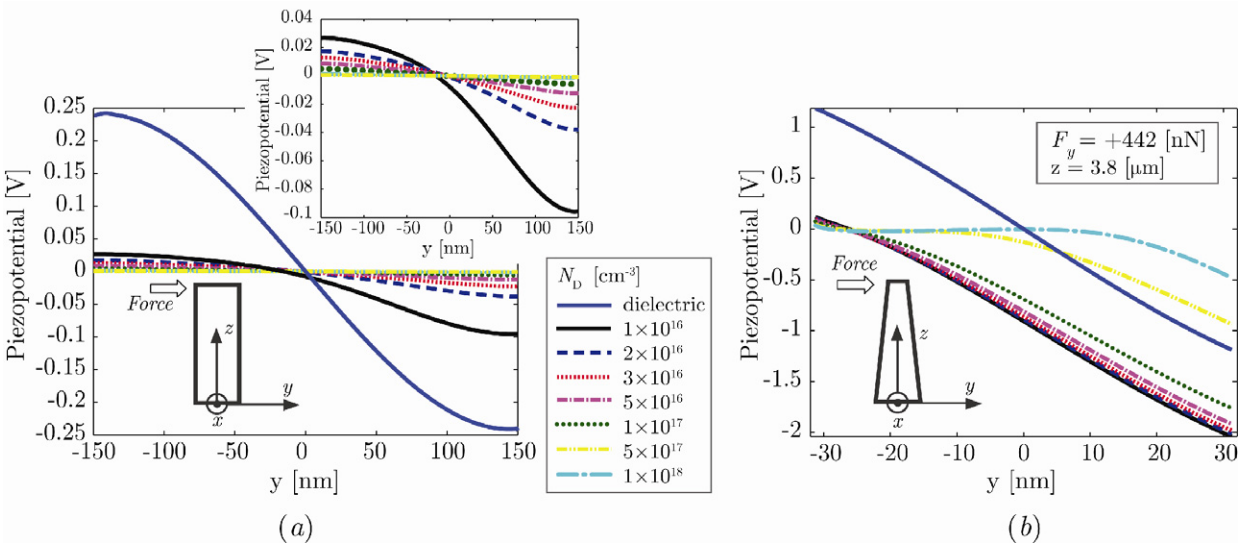

Figure 3. Piezopotentials in laterally bent cylindrical and conical nanowires as a function of $y(x = 0, z = 3.8\ \mu\text{m})$, for various n-type doping concentrations and for the dielectric case, with an external lateral force $F_y = 442$ nN, and $T = 300$ K. (a) Cylindrical nanowire. (b) Truncated conical nanowire; for doped nanowires the potential of the enhanced side of the tip is 'clamped' at 0 V and therefore results in a shift of the voltage to negative values only (n-type doping); the magnitude of the potential which can be extracted is therefore almost twice as large as for an hypothetical dielectric nanowire.

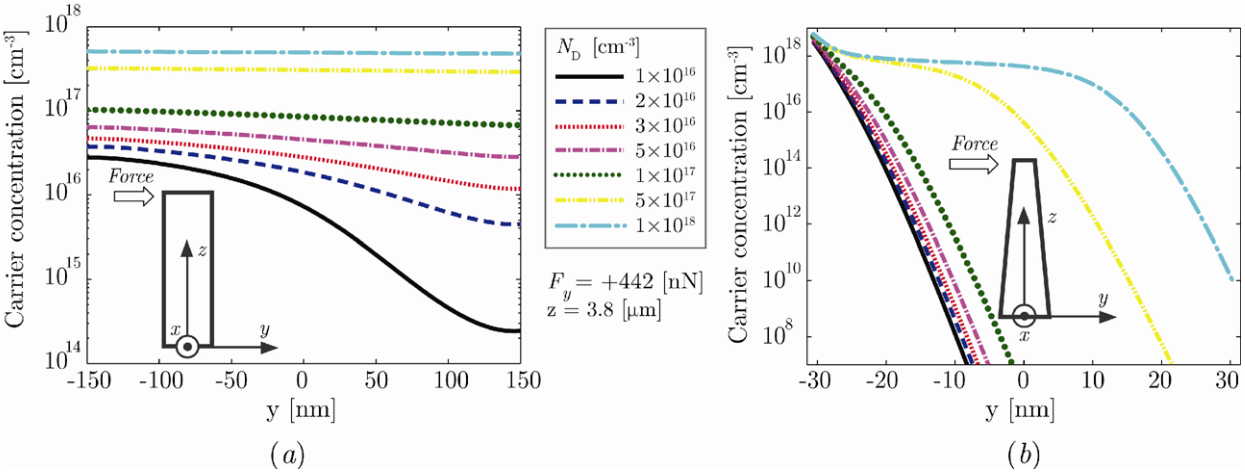

Figure 4. Electron carrier concentrations in laterally bent cylindrical and truncated conical ZnO nanowires as a function of y at $(x = 0, z = 3.8\ \mu\text{m})$ with various n-type doping levels, $T = 300$ K, and lateral force, $F_y = 442$ nN. (a) Cylindrical nanowire. (b) Truncated conical nanowire.

1.2. Doping-induced shift of the piezopotential

Figure 3 shows the piezoelectric potential for both the cylindrical and the truncated conical nanowires as a function of y at $(x = 0, z = 3.8\ \mu\text{m})$, with donor concentrations ranging from 10^{16} to 10^{18} cm^{-3}, external lateral force $F_y = 442$ nN, and $T = 300$ K; for the sake of comparison the cases of purely dielectric nanowires are also illustrated. For cylindrical nanowires the piezopotential in the dielectric case is much higher than for doped nanowires and therefore, for graphical clarity, is not shown in the inset. Consistently with [18, 20], in the case of cylindrical nanowires, the piezopotential is more and more screened at higher doping levels and, since we are only considering n-type doping (results with p-type doping can easily be found by duality, see above discussion), the negative voltages are much less reduced than the positive voltages and this asymmetry is more and more evident at higher doping levels. Obviously, the difference between the positive and the negative potentials (or, equivalently, between extended and compressed regions) is absent in the dielectric nanostructure whose piezopotential versus y-coordinate relationship is perfectly anti-symmetric.

Remarkably, for the considered level of lateral force, 442 nN, for cylindrical nanowires the voltage along the axis z is almost zero, as demonstrated by figure 1 for the axis z and by figure 2 for the point $z = 3.8\ \mu\text{m}, x = 0, y = 0$, so that the axis z almost perfectly separates the positive and the negative voltage regions; in contrast, with the same lateral force, the tip of the tapered nanowire is almost entirely a negative voltage region and, in the proximity of the tip, the

voltage along the axis z is negative. A crucial consequence is that in the case of the cylindrical nanowire both the depletion and enhancement are weak, due to the small magnitudes of the piezopotential and, therefore, the carrier concentration is almost uniform, whereas in the truncated conical nanowire the tip, apart for very high doping levels, is almost entirely depleted, as illustrated by figure 4, which shows the negative charge carrier concentrations in laterally bent cylindrical and conical nanowires along the axis ($x = 0, z = 3.8$ μm) and, in particular, shows, for the truncated conical nanowire, the strong enhancement in the very small positive voltage region as well as the strong depletion in almost the entire tip.

For the considered level of force, in cylindrical nanowires the piezopotential with typical doping levels is much smaller than for dielectric nanowires. In contrast and in disagreement with superficial expectations, unless doping levels are very high (e.g. 5×10^{17} cm^{-3} or higher, i.e. much higher than typical effective-donor concentrations, around 10^{17} cm^{-3} [18]) the magnitude of the output piezopotential for a doped conical nanowire is comparable or even higher than for a purely dielectric nanowire. In particular, figure 3(b) shows an almost-ideal voltage shift between the piezopotentials of doped and purely dielectric truncated conical nanowires. In fact, for a purely dielectric conical nanowire the equivalent piezoelectric charges are obviously located at the lateral surfaces of the nanowire so that, similar to a capacitor, the electric field within the nanowire is almost constant and orthogonal to the 'plates' (for simplicity, we neglect the bending of the 'plates') of the capacitor, resulting in a piezopotential which almost linearly depends on y (figure 3(b)). Additionally, similar to cylindrical dielectric nanowires [19], for truncated conical dielectric nanowires, the potential is zero along the z axis which separates the compressive and the tensile region, so that the piezopotential in dielectric conical nanowires is an anti-symmetric function of y. In contrast, in the case of n-type doped conical nanowires, positive voltages cannot be well preserved because of free electrons, and the maximum positive voltage at the compressed side of the tip must anyway be close to zero. However, since the strain is almost identical (the converse piezoelectric effect is typically negligible) to the case of the purely dielectric nanowire, the piezoelectric equivalent charges are almost the same. If, taking into account both the effective depletion of almost the entire tip (see figure 4) and the Gauss theorem, we travel close to the tip from the compressed region toward the extended region, we find an almost constant electric field and, therefore, by integration, a piezopotential almost linearly dependent on y and, by the Gauss theorem (the equivalent piezoelectric charges are almost the same as with the dielectric nanowire), an almost identical maximum voltage difference, with the only difference that the voltage at the extended wall of the nanowire (enhanced region) is almost zero due to the free electrons, which do not allow significant positive voltages. In conclusion, the piezopotential profile in the dielectric nanowire is almost the same as in the doped nanowire, with the only exception being an almost-ideal voltage shift of the piezopotential (which, for the dielectric nanowire, is zero along the z axis, i.e. for $y = 0$ and, for the doped nanowire, is close to zero in proximity to the extended wall of the nanowire).

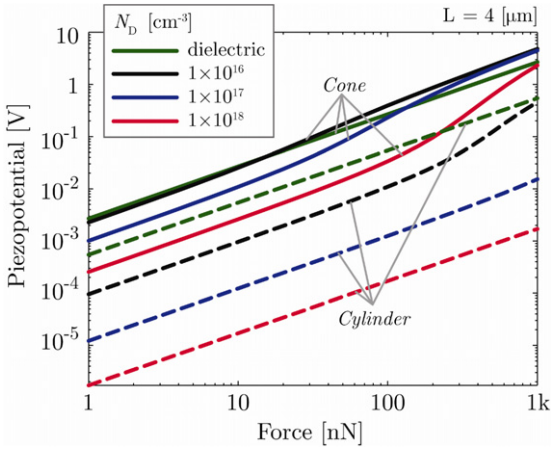

Figure 5. Output piezopotential (top electrode at $z = 3.8$ μm) for both the cylindrical and the truncated conical nanowires as a function of the external lateral force F_y, for various donor concentrations, and $T = 300$ K.

An impressive consequence is that the magnitude of the piezopotential that can be extracted from piezoelectric nanowires with typical (around 10^{17} cm^{-3}) doping levels can be even higher than from hypothetical nanowires without free charges (e.g. in figure 3(b), between -1.8 and -2 V for doping levels below 10^{17} cm^{-3} versus -1.3 V for a dielectric nanowire). In practice, at the nanoscale we can almost perfectly deplete the small tip of the tapered nanostructure with tiny forces, so that the total voltage difference from the compressed to the extended region is almost identical to the dielectric case. Moreover, the voltage of the enhanced side of the tip is 'clamped' at 0 V and therefore allows the voltage to shift only to negative values (n-type doping) or only to positive values (p-type doping), thus resulting in a maximum magnitude which is almost twice as large (similar to diode 'clampers' circuits).

1.3. Output piezopotential

For conciseness, we refer to the output piezopotential as the maximum magnitude of the piezopotential which can be extracted by an external contact in proximity to the tip when the total-bottom-electrode [19] is grounded. Moreover, taking into account that establishing a perfect contact exactly at the tip is obviously difficult, as well as in order to avoid distortions due to the method (i.e. force uniformly applied at the tip surface), similar to previous lateral bending calculations [17–19], we take the output piezopotential at 200 nm from the tip.

Figure 5 shows, for various n-type doping levels, with $T = 300$ K, for both the cylindrical and the truncated conical nanowires, with a grounded base contact [17–20], the output piezopotential as a function of the external lateral force F_y, assuming that the top electrode is at $z = 3.8$ μm (i.e. we consider a potential with a magnitude which is slightly lower

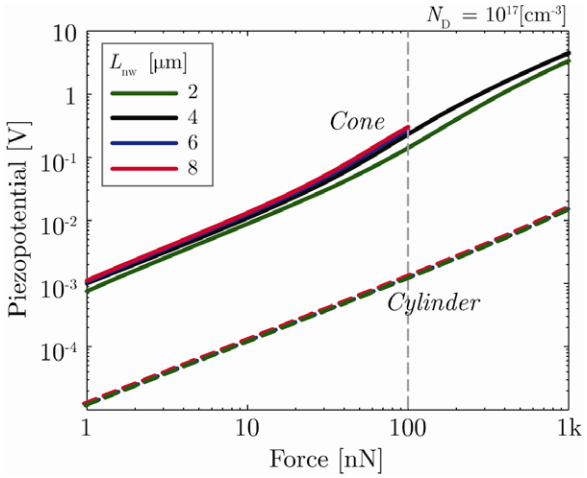

Figure 6. Output piezopotential (top electrode at 200 nm from the tip) from both the cylindrical and the truncated conical nanowires as a function of the external lateral force F_y, for various nanowires lengths, and $T = 300$ K (the curves for the tallest cone are truncated at strain levels above 3%, which would clearly require more complex mechanical models to take into account non-elastic effects).

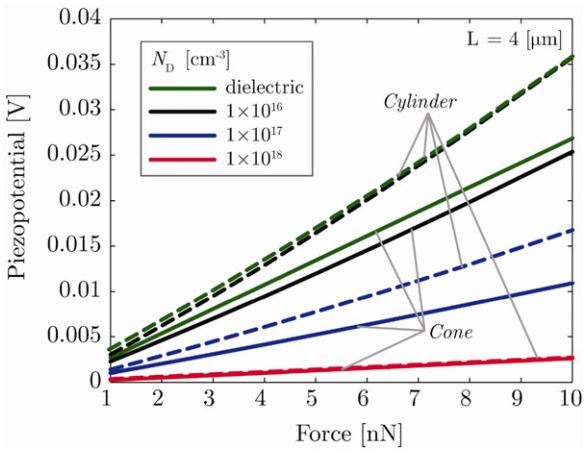

Figure 7. Output piezopotential (top electrode at $z = 3.8$ μm) for both a very thin cylindrical (R_{nw} equal to 25 nm) and a truncated conical ($R_{b,nw}$ and $R_{t,nw}$ equal to 150 nm and 25 nm, respectively) nanowire as a function of the external lateral force F_y, for various doping levels and $T = 300$ K; the force magnitude is limited to 10 nN in order to keep the strain in the thin cylindrical nanowire below about 3% (larger strains would require more complex, non-elastic models).

than at the tip, $z = 4$ μm). We stress that in cylindrical nanowires the highest magnitudes of the piezopotentials are found in internal regions close to the base, where the strain is maximum; however, these internal potentials, which are not accessible from external contacts, may not be extracted and, therefore, do not affect the output piezopotential (see definition above).

Under sufficiently small deformations, the strain linearly depends on force; until the force and, therefore, the piezopotential are small enough, the depletion and enhancement are weak and, therefore, the piezopotential linearly depends on strain. Consistently with figure 3(b), the piezopotential is reduced by doping only if the force cannot effectively deplete the tip. Clearly, for tapered nanowires (where, for a given input force, the strains are much higher) effective depletion is easily achieved at low force levels while, at substantially higher force levels, doped cylindrical nanowires also become more effective, because the piezopotential becomes so high that it can effectively deplete a significant part of the cylinder, but this requires much higher forces and, therefore, is only visible in figure 5 for very low (10^{16} cm^{-3}) doping levels. As a consequence of the almost-ideal voltage shift explained before, unless the doping level is very high, at sufficiently high forces the output piezopotential in doped conical nanowires is even higher than in hypothetical purely dielectric nanowires. As evident from figure 4, the magnitude of the piezopotential that can be extracted from deflected tapered nanowires may be orders of magnitude higher than for cylindrical nanowires. Besides, very small dimensions of the tip region are also likely to result in strong size effects (including piezoelectric coefficients [4, 5] and mechanical properties [42]) so that, similar to [22], piezopotentials higher than our predictions can be generated in tapered nanowires, an effect which in the absence of accurate data we preferred not to consider in our simulations.

Figure 6 shows the output piezopotential for both the cylindrical and the truncated conical nanowires as a function of the external lateral force for various nanowire lengths (top electrode at $z = 3.8$ μm). The curves for the tallest conical nanowire are truncated at 100 nN in order to avoid strain levels above 3%, which clearly would require more complex non-elastic mechanical models. As evident, the output piezopotential is almost independent of the height of the nanowires, consistent with previous studies on laterally deflected nanowires (independently of neglecting [17] or considering [18] free charges).

Clearly, as a consequence of scaling laws, if the diameter is reduced, small forces can also effectively deplete a cylindrical nanowire; for instance, with a diameter of 50 nm, a length of 600 nm, a lateral force of 80 nN [18] may already deplete the tip of a cylindrical nanowire. However, tapered nanostructures can also have crucial advantages over very thin cylindrical nanowires. Figure 7 shows the output piezopotential for both a very thin cylindrical (R_{nw} equal to 25 nm) and a truncated conical ($R_{b,nw}$ and $R_{t,nw}$ equal to 150 nm and 25 nm, respectively) nanowire as a function of the external lateral force F_y (top electrode at $z = 3.8$ μm), for various doping levels. Though, obviously, for a given input mechanical force the output piezopotential is higher in the thin cylindrical nanowire, this advantage is not extreme (e.g. for the typical doping level 10^{17} cm^{-3}, about 11 mV versus about 17 mV for 10 nN input force) and is likely associated with severe practical issues. In fact, the truncated conical shape is much easier to fabricate (the very thin cylindrical nanowire has an aspect ratio equal to 4 μm/25 nm, i.e. 160) and may have substantially improved mechanical robustness and stability; the very thin cylindrical nanowire would likely have a much weaker adhesion to the substrate (its base area is 36 times smaller) and would also be subject to extremely high strains at the base, with such high strains not being effective

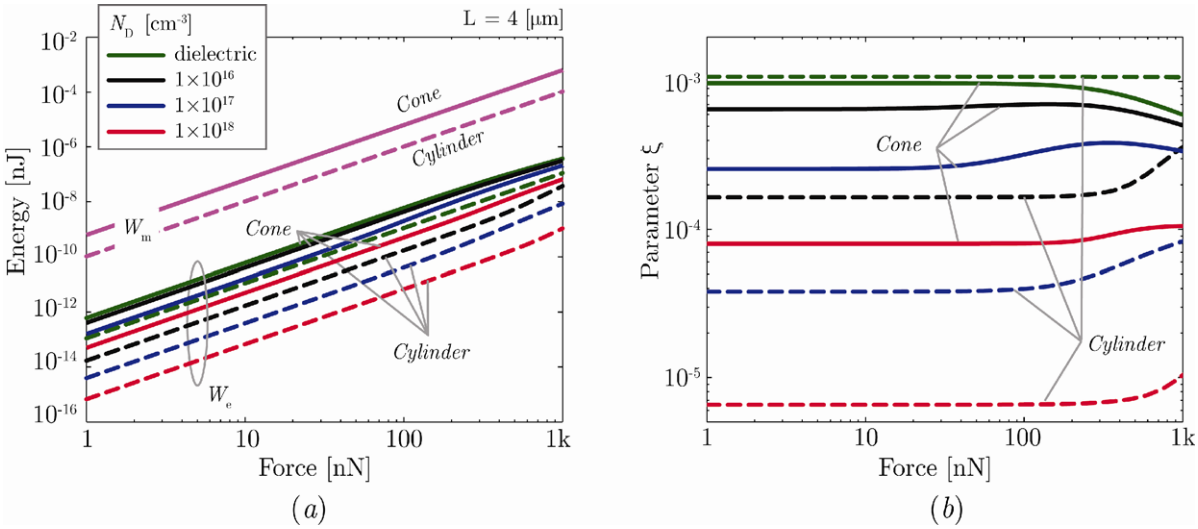

Figure 8. Stored energies and ξ for both the cylindrical and the truncated conical ZnO nanowires as a function of the external lateral force F_y, for various doping concentrations, and $T = 300$ K. (a) Stored mechanical energy (W_m) and stored electrostatic energy (W_e). (b) ξ.

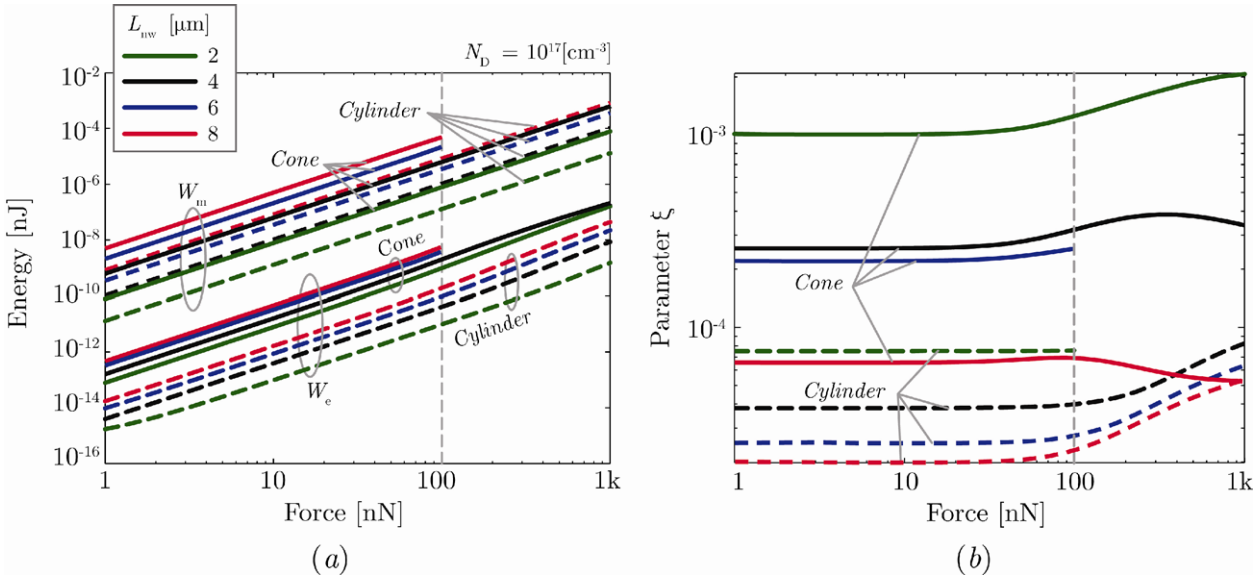

Figure 9. Stored energies and ξ for both the cylindrical and the truncated conical ZnO nanowires as a function of the external lateral force F_y, for various lengths, with doping level $N_D = 10^{17}$ cm^{-3}, and $T = 300$ K (curves truncated at strain levels above 3%, which would require nonlinear mechanical models). (a) Stored mechanical energy (W_m) and stored electrostatic energy (W_e). (b) ξ.

in the generation of a high piezopotential (because of the total bottom contact [19], which partially deactivates the base). In fact, the force magnitude in figure 7 is limited to values below 10 nN in order to keep the strain in the thin cylindrical nanowire below about 3% (larger strains would require more complex, non-elastic mechanical models), whereas forces up to 1 μN can be safely applied to the truncated conical nanowire without incurring such extreme strain levels, which may also degrade the reliability.

As shown in figure 7, in comparison with extremely thin cylindrical nanowires, the truncated conical shape can produce, in response to tiny input mechanical forces, almost the same piezopotentials with substantial advantages in terms of ease of fabrication, mechanical robustness, stability, and much smaller maximum strains within the nanowire for comparable levels of output potential.

1.4. ξ for laterally deflected nanowires

The parameter ξ has been defined [19, 22] as the ratio between the stored electrostatic energy W_e and the total (electrostatic and mechanical) stored energy $W_e + W_m$. Since it is currently impossible to theoretically evaluate the energy conversion efficiency of piezoelectric nano-devices (which would require to take into account, for instance, the process dynamics, the external load, and the parasitic impedances [19]), ξ [19, 22] can be used an upper limit to the efficiency of the static mechanical-to-electrical energy conversion process. In

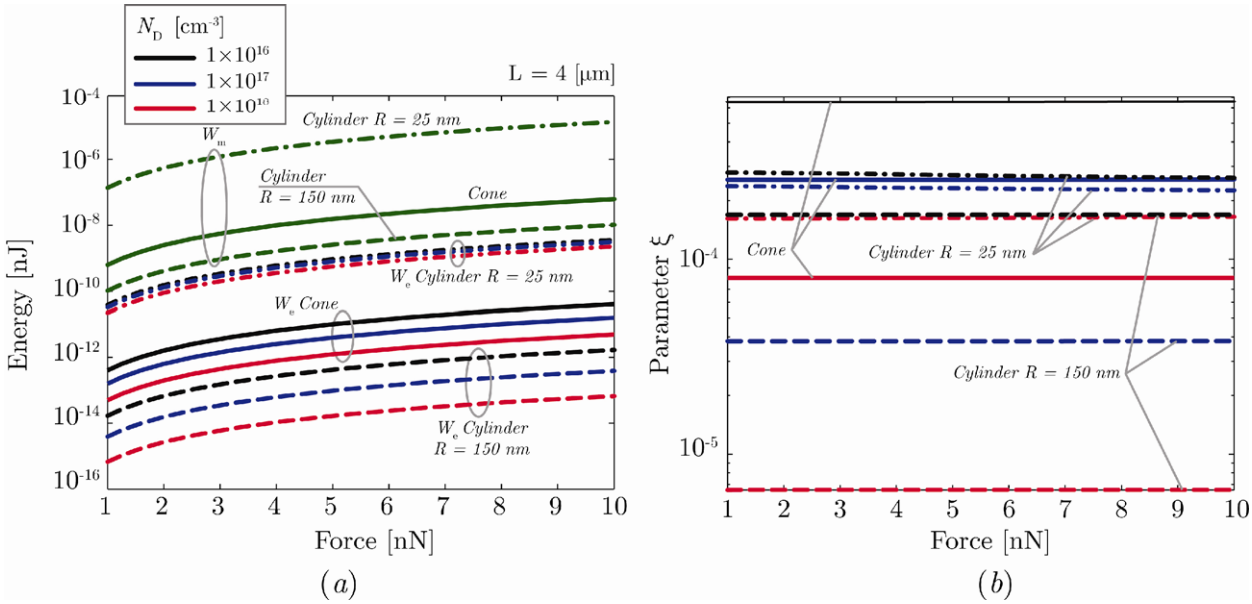

Figure 10. Stored energies and ξ for truncated conical, thin cylindrical (same diameter as the tip diameter of the truncated conical nanowire), and large cylindrical (same diameter as the base diameter of the truncated conical nanowire) ZnO nanowires as a function of the external lateral force F_y, for various doping levels, and $T = 300$ K. (a) Stored mechanical energy (W_m) and stored electrostatic energy (W_e). (b) ξ..

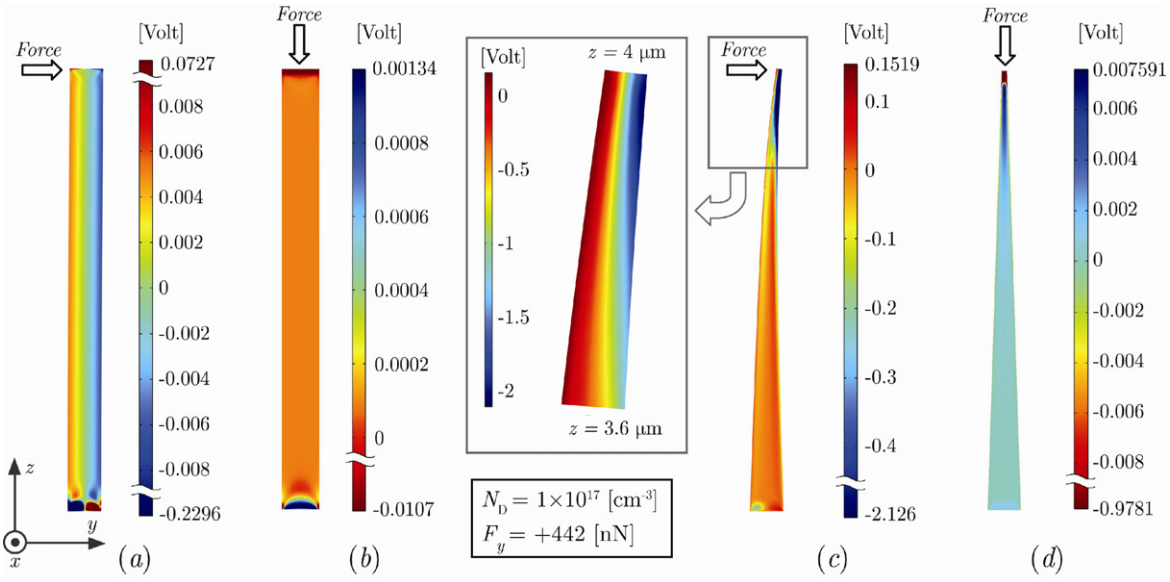

Figure 11. Color-maps of the piezopotential in laterally bent and vertically compressed, cylindrical and truncated conical n-type ZnO nanowires for the cross-section $x = 0$ with dopant concentration $N_D = 10^{17}$ cm^{-3}, $T = 300$ K, and lateral force, $F_y = 442$ nN; for graphical clarity some color bars are saturated. (a) Laterally bent cylindrical nanowire. (b) Vertically compressed cylindrical nanowire. (c) Laterally bent truncated conical nanowire (zoom in the inset). (d) Vertically compressed truncated conical nanowire.

previous studies, ξ was computed in the absence of free charges [19] or, when taking into account free charges, only for vertical compression [22].

Figure 8 shows, for various doping levels, the mechanical, W_m, and electrical, W_e, stored energies in laterally bent cylindrical and truncated conical nanowires as a function of the external lateral force F_y; for a given input force level, the mechanical energy stored in the laterally bent conical nanowire is higher than in the cylindrical nanowire due to the much higher displacement; moreover, consistently with the above discussion, in the case of cylindrical nanowires the presence of doping results in a much more severe reduction of the stored electrostatic energy. In all cases, except for hypothetical dielectric nanowires, ξ is significantly higher for conical nanowires.

Figure 9 shows the stored energies and ξ for both the cylindrical and the truncated conical nanowires as a function of the external lateral force F_y, for various nanowire lengths, and $T = 300$ K; for a given input force, at high lengths, the displacement is highly increased and, therefore, the stored mechanical energy is largely increased, thus reducing ξ.

Figure 10 shows the stored energies and ξ for the truncated conical, thin cylindrical (same diameter as the

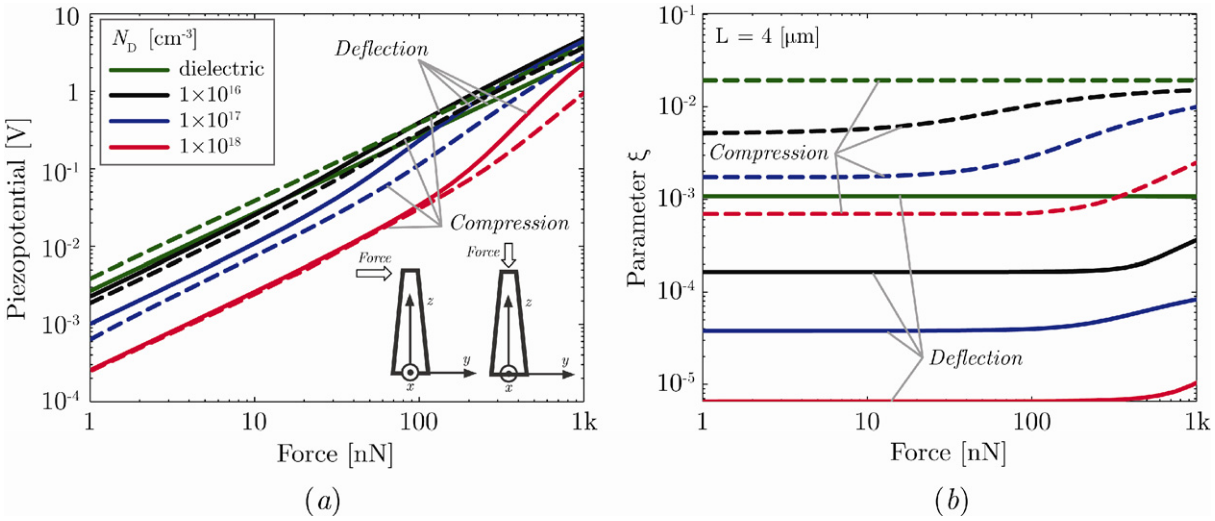

Figure 12. Comparison between vertical compression and lateral deflection of truncated conical ZnO nanowires ($R_{b,nw}$ and $R_{t,nw}$ equal to 150 nm and 25 nm, respectively) for various doping levels and $T = 300$ K. (a) Output piezopotential as a function of the external mechanical, compressive or deflecting, force F_y (assuming, for lateral deflection, the top electrode at $z = 3.8$ μm). (b) ξ as a function of the external mechanical, compressive or deflecting, force F_y.

tip diameter of the truncated conical nanowire), and large cylindrical (same diameter as the base diameter of the truncated conical nanowire) ZnO nanowires as a function of the external lateral force F_y, for various doping levels, and $T = 300$ K; we observe that ξ for conical nanowires, for some doping levels, is even higher than for the thin cylindrical nanowire, due to the very large strain (i.e. very high stored mechanical energy) in the thin nanowire; similar to figure 7, the force is limited to values below 10 nN in order to keep the strain in the thin cylindrical nanowire below about 3%.

1.5. Comparison between vertical compression and lateral bending

Figure 11 shows the color-maps of the piezopotential in laterally bent and vertically compressed, cylindrical and truncated conical n-type ZnO nanowires for the cross-section $x = 0$ with dopant concentration $N_D = 10^{17}$ cm^{-3}, $T = 300$ K, and lateral force, $F_y = 442$ nN. As evident, in contrast with the case of constant-cross-section nanowires, with tapered quasi-1D nanostructures, lateral deflection may offer a higher piezopotential than vertical compression, with the additional decisive advantage of no buckling issues (in the case of a vertical compressive force, above a certain strain there will be deviations from a purely vertical compression, i.e. buckling). In fact, in the case of a laterally bent conical nanowire, if the tip is sufficiently sharp, for a given magnitude of the mechanical force, a strain larger than the strain obtained by vertical compression can be easily generated by a small bending force and, contrary to the laterally bent cylindrical structures, high strains are also generated in regions far from the nanowire base (and, therefore, in regions which are not partially disabled by the total bottom contact at the base). In contrast, for the laterally deflected cylindrical nanowire, high piezopotentials are only generated in internal regions close to the base (i.e. where the strain is maximum) and are not accessible by external contacts.

For completeness, figure 11 also shows a zoom of the laterally deflected tapered nanowire (with z ranging from 3.6 μm to the tip, at 4 μm), thus confirming that high piezopotentials can be found even a few hundred nanometers from the tip (e.g. see the corresponding color map of the piezopotential for the cross-sections $z = 3.8$ μm in figure 2). We stress that, when transducing a mechanical force into a piezopotential using quasi-1D nanostructures, the possibility to use vertical compression may also be severely compromised by buckling issues, which in practice may restrict the system to very small input mechanical forces (or, equivalently, may severely limit the dynamic range for the input mechanical forces).

Figure 12 shows the output piezopotential for both vertical compression and lateral bending of a truncated conical ($R_{b,nw}$ and $R_{t,nw}$ equal to 150 nm and 25 nm, respectively) ZnO nanowire as a function of the external lateral force F_y, for various doping levels as well as the ξ-parameter. Apart from the dielectric case, lateral bending is superior in terms of the piezopotential and, therefore, may be preferable for piezotronics, piezo-phototronics, mechanical sensing, and piezo-controlled chemical reactions, especially when taking into account that with vertical compression the input dynamic range may be severely limited by buckling issues. However, consistently with predictions in [19] (obtained without considering free charges), vertical compression offers higher values of ξ and is therefore likely preferable for piezoelectric energy harvesting, also taking into account that with vertical compression it is easier to provide reliable electrical contacts to a large array of aligned nanowires [13].

2. Conclusions

We have confirmed that lateral bending is likely not optimal for energy harvesting; however, lateral bending of tapered piezo-semiconductive nanostructures can be ideal, with typical doping levels, for transducing tiny input mechanical forces into high and accessible piezopotentials, without the buckling issues associated with vertical compression.

Contrary to superficial expectations, we have also found that, in laterally bent tapered nanostructures, typical doping levels not only do not reduce, but can even increase, by up to two times, the output piezopotential, thus constituting an exception to the apparently obvious reduction of the output potential induced by free charges; this effect, which can be triggered by minuscule forces as a result of downscaling and of the tapered shape, is due to the combination of an effective tip depletion and of the 'clamped' voltage in the small enhanced part of the tip.

Our results may provide guidelines for designing high-performance piezo-nano-devices for mechanical sensing, energy harvesting, piezotronics, piezo-phototronics, and piezo-controlled chemical reactions, among others.

Acknowledgments

This work has been supported by the Italian Institute of Technology (Project Seed 'API NANE') and by the Italian Ministry for University and Research (FIRB—Futuro in Ricerca 2010 Project 'Nanogeneratori di ossido di zinco ad altissima efficienza per l'alimentazione di microsistemi impiantabili e di reti wireless di sensori').

Appendix. Details on the calculations

For our calculations, similar to previous works [17, 18, 20–22] we use a system of fully coupled nonlinear partial differential equations. The elastic behavior of piezoelectric media is governed by Newton's law

$$\nabla \cdot \sigma = 0, \tag{A.1}$$

where $\sigma = \sigma_{i,j} e_i \otimes e_j$ is the Cauchy stress tensor, while the piezopotential is governed by

$$\nabla \cdot D = q(N_{\mathrm{D}}^{+} + p - N_{\mathrm{A}}^{-} - n) \tag{A.2}$$

which is a form of Poisson's equation, where $D = D_j e_j$ is the vector of dielectric displacement, q is used to indicate the absolute value of the electronic charge, N_{D}^{+} and N_{A}^{-} are the ionized donor and acceptor concentrations, respectively, p is the free (mobile) hole concentration in the valence band and n is the free electron concentration in the conduction band. Since ZnO nanostructures typically show an n-type behavior we focus on n-type doping and consider $p = N_{\mathrm{A}}^{-} \cong 0$; however, since p-type ZnO nanowires have also been reported [29], we have also performed simulations of p-type nanowires using $n = N_{\mathrm{D}}^{+} \cong 0$, see below for discussion.

The two equations (A.1)–(A.2) are fully coupled by the constitutive equations relating mechanical and electrical quantities in piezoelectric media, i.e.,

$$\begin{aligned} \sigma_{i,j} &= c_{ijkl}^{\mathrm{E}} \varepsilon_{kl} - e_{kij} E_k \\ D_j &= e_{jkl} \varepsilon_{kl} + \kappa_0 \kappa_{jk}^{\varepsilon} E_k, \end{aligned} \tag{A.3}$$

where c_{ijkl}^{E}, e_{kij}, $\kappa_{jk}^{\varepsilon}$ are the elastic, piezoelectric and dielectric tensors, respectively (repeated summation index convention), E_k is the electric field and ε_{kl} is the strain tensor. According to the Fermi–Dirac statistics (due to the large strain of the nanowire, the band deformation can be important and ZnO can behave as a degenerate semiconductor) the carrier densities n and p are determined under thermodynamic equilibrium by the position of the Fermi level $\mathcal{E}_{\mathrm{F}}$ with respect to the conduction band edge $\mathcal{E}_{\mathrm{c}}$ and the valence band $\mathcal{E}_{\mathrm{v}}$. The densities can thus be calculated as,

$$n = N_{\mathrm{c}} \frac{2}{\sqrt{\pi}} F_{1/2}\left(\frac{\mathcal{E}_{\mathrm{F}} - \mathcal{E}_{\mathrm{c}}}{k_{\mathrm{B}} T}\right) \tag{A.4a}$$

$$p = N_{\mathrm{v}} \frac{2}{\sqrt{\pi}} F_{1/2}\left(\frac{\mathcal{E}_{\mathrm{v}} - \mathcal{E}_{\mathrm{F}}}{k_{\mathrm{B}} T}\right) \tag{A.4b}$$

where the equations (A.4*a*) and (A.4*b*) are used for n-type and p-type doping, respectively, $F_{1/2}(\cdot)$ is the Fermi integral (approximated in our numerical computations by means of the Joyce–Dixon approximation for reducing the CPU time), $N_{\mathrm{v}} = 2(\frac{2\pi m_{\mathrm{h}} k_{\mathrm{B}} T}{h^2})^{\frac{3}{2}}$ and $N_{\mathrm{c}} = 2(\frac{2\pi m_{\mathrm{e}} k_{\mathrm{B}} T}{h^2})^{\frac{3}{2}}$ are the effective density of states in the valence and conduction bands, respectively, T is the absolute temperature, k_{B} is the Boltzmann constant, h is the Planck constant, m_{e} is the effective mass of conduction band electrons and m_{h} is the effective mass of valence band holes.

In general, the ionized acceptor and donor concentrations are given by

$$N_{\mathrm{A}}^{-} = \frac{N_{\mathrm{A}}}{1 + g_{\mathrm{A}} \exp\left(\frac{\mathcal{E}_{\mathrm{A}} - \mathcal{E}_{\mathrm{F}}}{k_{\mathrm{B}} T}\right)}, \tag{A.5a}$$

$$N_{\mathrm{D}}^{+} = \frac{N_{\mathrm{D}}}{1 + g_{\mathrm{D}} \exp\left(\frac{\mathcal{E}_{\mathrm{F}} - \mathcal{E}_{\mathrm{D}}}{k_{\mathrm{B}} T}\right)}, \tag{A.5b}$$

where g_{A} and g_{D} are the ground-state degeneracy of the acceptor and donor impurity levels (usually $g_{\mathrm{A}} = g_{\mathrm{D}} = 2$) while $\mathcal{E}_{\mathrm{A}}$ and $\mathcal{E}_{\mathrm{D}}$ are the energy of the states introduced by acceptors and donors.

The conduction $\mathcal{E}_{\mathrm{c0}}$ and valence $\mathcal{E}_{\mathrm{v0}}$ band levels of a free-standing undeformed NW can be computed with reference to the Fermi level $\mathcal{E}_{\mathrm{F}}$, which is set to zero as reference, enforcing the neutrality conditions $N_{\mathrm{D}}^{+} + p = N_{\mathrm{A}}^{-} + n$. For a n-type semiconductor the equation $N_{\mathrm{D}}^{+} = n$ leads to

$$\mathcal{E}_{\mathrm{c0}} = k_{\mathrm{B}} T \ln\left(\frac{N_{\mathrm{c}} + \sqrt{N_{\mathrm{c}}^2 + 4 g_{\mathrm{D}} N_{\mathrm{c}} N_{\mathrm{D}} e^{\frac{\triangle \mathcal{E}_{\mathrm{D}}}{k_{\mathrm{B}} T}}}}{2 N_{\mathrm{D}}}\right), \tag{A.6a}$$

while for a p-type semiconductor the equation $p = N_{\mathrm{A}}^{-}$ leads to

$$\mathcal{E}_{\mathrm{v0}} = k_{\mathrm{B}} T \ln\left(\frac{-N_{\mathrm{v}} + \sqrt{N_{\mathrm{v}}^2 + 4 g_{\mathrm{A}} N_{\mathrm{v}} N_{\mathrm{A}} \mathrm{e}^{\frac{-\triangle \mathcal{E}_{\mathrm{A}}}{k_{\mathrm{B}} T}}}}{2 g_{\mathrm{A}} N_{\mathrm{v}} e^{\frac{\triangle \mathcal{E}_{\mathrm{A}}}{k_{\mathrm{B}} T}}}}\right), \tag{A.6b}$$

where $\mathcal{E}_D = \mathcal{E}_{c0} - \triangle\mathcal{E}_D$ and $\mathcal{E}_A = \mathcal{E}_{v0} + \triangle\mathcal{E}_A$ are the levels of acceptor and donor concentrations.

When the ZnO NW is deflected the valence and conduction band levels become a function of space coordinates $\mathbf{x}$, i.e. $\mathcal{E}_v(\mathbf{x})$ and $\mathcal{E}_c(\mathbf{x})$. In particular, the band edge shift $\triangle\mathcal{E}(\mathbf{x})$ is the sum of the electrostatic energy part qV and the deformation potential part $\triangle E_{def}$ (which may be important due to the large strain), i.e.

$$\begin{aligned}\triangle\,\mathcal{E}(\mathbf{x}) &= \mathcal{E}_c(\mathbf{x}) - \mathcal{E}_{c0} \\ &= \mathcal{E}_v(\mathbf{x}) - \mathcal{E}_{v0} = -qV + a_{def}\frac{\triangle v}{v_0}, \end{aligned} \tag{A.7}$$

where V is the electrostatic potential, and $a_{def}\frac{\triangle v}{v_0}$ is the band edge shift due to the deformation, which is proportional to the relative volume change $\frac{\triangle v}{v_0}$ through the deformation potential constant a_{def}. Finally, also the activation process of the donors and acceptors is modified by the deformation of the conduction and valence band edge. In fact, in equations (A.6) the acceptor energy level is given by $\mathcal{E}_A(\mathbf{x}) = \mathcal{E}_v(\mathbf{x}) + \triangle\mathcal{E}_A$, while the donor energy level is $\mathcal{E}_D(\mathbf{x}) = \mathcal{E}_c(\mathbf{x}) - \triangle\mathcal{E}_D$ (for simplicity we assume the band gap energy $\mathcal{E}_g$ remains constant).

Since the piezoelectric-semiconductor equations constitute a coupled nonlinear set, it is not possible to obtain a solution in one step, but a nonlinear iteration method must be used. As to the choice of the independent variables, we solve the coupled electro-mechanical problem for the variables $(\mathbf{u}, V)$, where $\mathbf{u}$ is the displacement vector in the spatial description (Eulerian form). As a result, the electric field is found by $\mathbf{E} = -\nabla V$, while the mechanical strain vector is related to the mechanical displacement by $\boldsymbol{\varepsilon} = [\mathbf{B}]\mathbf{u}$, where $[\mathbf{B}]$ is the strain–displacement matrix. By using the independent variables $(\mathbf{u}, V)$, equations (A.1)–(A.3) can be rewritten to obtain the coupled nonlinear partial differential equations as

$$\nabla \cdot \{[\mathbf{c}^E][\mathbf{B}]\mathbf{u} + [\mathbf{e}]^T\nabla V\} = 0 \tag{A.8a}$$

$$\nabla \cdot \{[\mathbf{e}][\mathbf{B}]\mathbf{u} - \kappa_0[\boldsymbol{\kappa}^\varepsilon]\nabla V\} = q(N_D^+ + p - N_A^- - n), \tag{A.8b}$$

where the impurities and the mobile charge densities are linked to the electrical potential V and the displacement $\mathbf{u}$ through equations (A.4), (A.5), (A.7), which are clearly the nonlinear terms of the equation system. In order to make the solution of equations (A.8) more efficient and to avoid possible numerical overflow and underflow errors, it is advisable to perform calculations using normalized quantities through a consistent scaling. The system of equations (A.8) has been solved through a standard Finite Element Method in conjunction with the damped iterative Newton method to deal with the nonlinearity. Taking advantage of the plane symmetry of the structure, we restricted the simulation to a half space ($x > 0$) and imposed equal to zero any derivative with respect to the variable on the plane xy. A nodal approach with second-order Lagrangian basis functions defined on a tetrahedral mesh has been used.

The simulation domain comprises the NW surrounded by air. We assumed a ZnO NW epitaxially grown along the c-axis (aligned with the z-axis) on a single crystal substrate and pushed by a force exerted at its tip directed along the y-axis. The NW is modeled as a simple cylinder oriented along the z-axis. Inside the NW the coupled piezoelectric model has been solved, while the simple Laplace equation $\nabla^2 V = 0$ has been enforced in the surrounding open space (considered as a non-solid medium). The infinite open space has been simulated by means of the second-order local Bayliss–Gunzburger–Turkel (BGT) [43] absorbing boundary conditions enforced on the outer boundary of the simulation domain.

The values of the ZnO parameters used in our calculations are as follows: the stiffness constants of ZnO are (for conciseness, the symmetries are not explicitly indicated) $c^E_{1111} = 209.7$ (GPa), $c^E_{3333} = 210.9$ (GPa), $c^E_{1122} = 121.1$ (GPa), $c^E_{2233} = 105.1$ (GPa), $c^E_{2323} = 42.47$ (GPa), $c^E_{1212} = 44.29$ (GPa) [44]; the piezoelectric constants are $e_{311} = e_{322} = -0.51$ (C m^{-2}), $e_{333} = 1.22$ (C m^{-2}), $e_{113} = e_{223} = -0.45$ (C m^{-2}) [45]; the dielectric relative permittivity constants are $\kappa^\varepsilon_{11} = \kappa^\varepsilon_{22} = 7.77$ and $\kappa^\varepsilon_{33} = 8.91$ [46]; the effective electron mass is $m_e = 0.28m_0$ [47], with m_0 the free electron mass; the deformation potential constant is $a_c = -6.05$ (eV) [48]; the distance between the donor (acceptor) energy level and conduction (valence) band is $\triangle\mathcal{E}_D = \triangle\mathcal{E}_A = 35$ (meV) [46]; the temperature is $T = 300$ (K); the band gap is $\mathcal{E}_g = 3.4$ (eV).

References

[1] Wang Z L and Song J 2006 Piezoelectric nanogenerators based on zinc oxide nanowire arrays *Science* **312** 242–6

[2] Wang Z L 2012 Progress in piezotronics and piezo-phototronics *Adv. Mater.* **24** 4632–46

[3] Starr M B, Shi J and Wang X 2012 Piezopotential-driven redox reactions at the surface of piezoelectric materials *Angew. Chem. Int. Edn Engl.* **51** 5962–6

[4] Agrawal R and Espinosa H D 2011 Giant piezoelectric size effects in zinc oxide and gallium nitride nanowires. A first principles investigation *Nano Lett.* **11** 786–90

[5] Espinosa H D, Bernal R A and Minary-Jolandan M 2012 A review of mechanical and electromechanical properties of piezoelectric nanowires *Adv. Mater.* **24** 4656–75

[6] Hughes W L and Wang Z L 2005 Controlled synthesis and manipulation of ZnO nanorings and nanobows *Appl. Phys. Lett.* **86** 043106

[7] Xu S, Hansen B J and Wang Z L 2010 Piezoelectric-nanowire-enabled power source for driving wireless microelectronics *Nature Commun.* **1** 93

[8] Hu Y, Zhang Y, Xu C, Lin L, Snyder R L and Wang Z L 2011 Self-powered system with wireless data transmission *Nano Lett.* **11** 2572–7

[9] Zhu G, Wang A C, Liu Y, Zhou Y and Wang Z L 2012 Functional electrical stimulation by nanogenerator with 58 V output voltage *Nano Lett.* **12** 3086–90

[10] Cha S N, Seo J S, Kim S M, Kim H J, Park J Y, Kim S W and Kim J M 2010 Sound-driven piezoelectric nanowire-based nanogenerators *Adv. Mater.* **22** 4726–30

[11] Lee K Y, Kumar B, Seo J, Kim K-H, Sohn J I, Cha S N, Choi D, Wang Z L and Kim S 2012 p-type polymer-hybridized high-performance piezoelectric nanogenerators *Nano Lett.* **12** 1959–64

[12] Kim K-H, Lee K Y, Seo J, Kumar B and Kim S 2011 Paper-based piezoelectric nanogenerators with high thermal stability *Small* **7** 2577–80

[13] Xu S, Qin Y, Xu C, Wei Y, Yang R and Wang Z L 2010 Self-powered nanowire devices *Nature Nanotechnol.* **5** 366–73

[14] Wang X, Song J, Liu J and Wang Z L 2007 Direct-current nanogenerator driven by ultrasonic waves *Science* **316** 102–5

[15] Yang S, Wang L, Tian X, Xu Z, Wang W, Bai X and Wang E 2012 The piezotronic effect of zinc oxide nanowires studied by *in situ* TEM *Adv. Mater.* **24** 4676–82

[16] Wang L, Tian X, Yang S, Xu Z, Wang W and Bai X 2012 Dynamic nanomechanics of zinc oxide nanowires *Appl. Phys. Lett.* **100** 163110

[17] Gao Y and Wang Z L 2007 Electrostatic potential in a bent piezoelectric nanowire. The fundamental theory of nanogenerator and nanopiezotronics *Nano. Lett.* **7** 2499–505

[18] Gao Y, Wang Z L and Georgia A 2009 Equilibrium potential of free charge carriers in a bent piezoelectric semiconductive nanowire *Nano. Lett.* **9** 1103–10

[19] Falconi C, Mantini G, D'Amico A and Wang Z L 2009 Studying piezoelectric nanowires and nanowalls for energy harvesting *Sensors Actuators* B **139** 511–9

[20] Mantini G, Gao Y, D'Amico A, Falconi C and Wang Z L 2009 Equilibrium piezoelectric potential distribution in a deformed ZnO nanowire *Nano Res.* **2** 624–9

[21] Romano G, Mantini G, Di Carlo A, D'Amico A, Falconi C and Wang Z L 2011 Piezoelectric potential in vertically aligned nanowires for high output nanogenerators *Nanotechnology* **22** 465401

[22] Araneo R, Lovat G, Burghignoli P and Falconi C 2012 Piezo-semiconductive quasi-1D nanodevices with or without anti-symmetry *Adv. Mater.* **24** 4719–24

[23] Sun C, Shi J and Wang X 2010 Fundamental study of mechanical energy harvesting using piezoelectric nanostructures *J. Appl. Phys.* **108** 034309

[24] Zhu G, Yang R, Wang S and Wang Z L 2010 Flexible high-output nanogenerator based on lateral ZnO nanowire array *Nano Lett.* **10** 3151–5

[25] Lin Y-F, Song J, Ding Y, Lu S-Y and Wang Z L 2008 Alternating the output of a CdS nanowire nanogenerator by a white-light-stimulated optoelectronic effect *Adv. Mater.* **20** 3127–30

[26] Lin Y-F, Song J, Ding Y, Lu S-Y and Wang Z L 2008 Piezoelectric nanogenerator using CdS nanowires *Appl. Phys. Lett.* **92** 022105

[27] Song J, Wang X, Liu J, Liu H, Li Y and Wang Z L 2008 Piezoelectric potential output from ZnO nanowire functionalized with p-type oligomer *Nano Lett.* **8** 203–7

[28] Lin S S, Song J H, Lu Y F and Wang Z L 2009 Identifying individual n-and p-type ZnO nanowires by the output voltage sign of piezoelectric nanogenerator *Nanotechnology* **20** 1–5

[29] Lu M, Song J, Lu M, Gao Y, Chen L, Wang Z L and Chen M 2009 Piezoelectric nanogenerator using p-type ZnO nanowire arrays *Nano Lett.* **9** 1223–7

[30] Huang C-T, Song J, Tsai C-M, Lee W-F, Lien D-H, Gao Z, Hao Y, Chen L-J and Wang Z L 2010 Single-InN-nanowire nanogenerator with upto 1 V output voltage *Adv. Mater.* **22** 4008–13

[31] Huang C-T, Song J, Lee W-F, Ding Y, Gao Z, Hao Y, Chen L-J and Wang Z L 2010 GaN nanowire arrays for high-output nanogenerators *J. Am. Chem. Soc.* **132** 4766–71

[32] Wang X, Song J, Zhang F, He C, Hu Z and Wang Z 2010 Electricity generation based on one-dimensional group-III nitride nanomaterials *Adv. Mater.* **22** 2155–8

[33] Zhou Y S *et al* 2012 Nano-Newton transverse force sensor using a vertical gan nanowire based on the piezotronic effect *Adv. Mater* **25** 883–8

[34] Chen C-Y, Liu T-H, Zhou Y, Zhang Y, Chueh Y-L, Chu Y-H, He J-H and Wang Z L 2012 Electricity generation based on vertically aligned $PbZr_{0.2}Ti_{0.8}O_3$ nanowire arrays *Nano Energy* **1** 424–8

[35] Chen C-Y, Zhu G, Hu Y, Yu J-W, Song J, Kai-Yuan C, Luing-Han P, Li-Jen C and Zhong-lin W 2012 Gallium nitride nanowire based nanogenerators and light-emitting diodes *ACS Nano* **6** 5687–92

[36] Riaz M, Song J, Nur O, Wang Z L and Willander M 2011 Study of the piezoelectric power generation of ZnO nanowire arrays grown by different methods *Adv. Funct. Mater.* **21** 628–33

[37] Perlasamy C and Chakrabarti P 2011 Time dependent degradation of Pt/ZnO nanoneedle rectifying contact based piezoelectric nanogenerator *J. Appl. Phys.* **109** 054306

[38] Park S-S, Lee J-M, Kim S-J, Kim S-H, Kim S-W, Yi M-S, Maeng S and Fujita S 2008 ZnO nanotips and nanorods on carbon nanotube/Si substrates: anomalous p-type like optical properties of undoped ZnO nanotips *Nanotechnology* **19** 245708

[39] Wang X, Ding Y, Yuan D, Hong J-I, Liu Y, Wong C P, Hu C and Wang Z L 2012 Reshaping the tips of ZnO nanowires by pulsed laser irradiation *Nano Res.* **5** 412–20

[40] Cho S, Lee B R, Kim H, Park D and Lee K 2009 Synthesis of density-controlled ZnO nanoneedle arrays on a flexible substrate by addition of Al salts and use of microwave irradiation *Mater. Lett.* **63** 2025–8

[41] Wen X, Wu W, Ding Y and Wang Z L 2012 Seedless synthesis of patterned ZnO nanowire arrays on metal thin films (Au, Ag, Cu, Sn) and their application for flexible electromechanical sensing *J. Mater. Chem.* **22** 9469–76

[42] Asthana A, Momeni K, Prasad A, Yap Y K and Yassar R S 2011 *In situ* observation of size-scale effects on the mechanical properties of ZnO nanowires *Nanotechnology* **22** 265712

[43] Bayliss A, Gunzburger M A X and Turkel E L I 1982 Boundary conditions for the numerical solution of elliptic equations in exterior regions *SIAM J. Appl. Math.* **42** 430–51

[44] Bateman T B 1962 Elastic moduli of single-crystal zinc oxide *J. Appl. Phys.* **33** 3309–12

[45] Carlotti G, Socino G, Petri A and Verona E 1987 Acoustic investigation of the elastic properties of ZnO films *Appl. Phys. Lett.* **51** 1889–91

[46] Ashkenov N *et al* 2003 Infrared dielectric functions and phonon modes of high-quality ZnO films *J. Appl. Phys.* **93** 126

[47] Xu Y and Ching W Y 1993 Electronic, optical, and structural properties of some wurtzite crystals *Phys. Rev.* B **48** 4335–51

[48] Shan W, Walukiewicz W, Ager J W III, Yu K M, Zhang Y, Mao S S, Kling R, Kirchner C and Waag A 2005 Pressure-dependent photoluminescence study of ZnO nanowires *Appl. Phys. Lett.* **86** 1–4